This article has been accepted for publication in a future issue of this journal, but has not been fully edited. Content may change prior to final publication. Citation information: DOI 10.1109/TMAG.2017.2703653, IEEE Transactions on Magnetics

An Algorithm for Transmitter Optimization in Electromagnetic Tracking Systems

Mohd Noor Islam, Andrew J. Fleming
School of Electrical Engineering and Computer Science
The University of Newcastle
Callaghan, Australia

Electromagnetic (EM) tracking systems are used extensively in biomedical devices, gaming consoles, and animation because they are inexpensive and do not require line of sight. However, the measurement range is limited by the amplitude of the induced voltage in the sensing coil. The induced voltage is a function of the transmitter parameters such as the coil dimensions, signal power and frequency. The transmitted power is typically restricted by the physical constraints in the application. This article develops an algorithm to optimize the dimensions of the transmitting coil for maximum induced voltage. The proposed method is suitable for a transmitter consisting of three concentric, orthogonal transmitting coils of the type commonly used in 6-DOF localization. Simulation and experimental results are presented which demonstrate the efficacy of the proposed method.

Index Terms—**Electromagnetic (EM) tracking system, Transmitting coil, Sensing Coil.**

I. Introduction

A Six-degree-of-freedom (6-DOF) electromagnetic (EM) tracking system is composed of three concentric, orthogonal transmitting and sensing coils [1]–[12]. The transmitting coils are excited by AC signals to create magnetic dipoles which induce voltage in the sensing coils. EM systems are extensively used in applications such as catheter and endoscope tracking [13]–[22], helmet tracking in the military [21], real time motion tracking in games and the film industry [23], flight simulation, and virtual reality. EM tracking systems are inexpensive and do not require line of sight.

Although EM systems have many advantageous characteristics, the measurement range is limited by the dramatic signal attenuation in space [2], [15], [18]. The sensitivity and range can be increased by increasing the signal power, optimizing the sensing coils [24], [25], and/or optimizing the transmitting coils. This article develops an algorithm for optimizing the transmitting coil dimensions for a given power level.

Signal frequency has a major impact on the transmitter optimization. Commercially available tracking systems use a low frequency signal (e.g. as 25 Hz [26], 120 Hz [21] or 144 Hz [22]). These frequencies minimize any distortion created by nearby metallic objects. However, low frequencies also limit the measurement rate [26] and may be susceptible to mains interference [27]. On the other hand, by increasing the frequency, resonance coupling [15] can be implemented, which increases the sensitivity of the sensing circuit. The distortion effect can be compensated by using a calibration technique [28]. This article demonstrates that higher frequencies result in lower mass and greater sensitivity and range. The maximum signal frequency is limited by the proximity of metal objects and, for example, the loss due to body tissue which increases sharply above 1 MHz [29] .

The proposed algorithm is demonstrated for an example transmitter where the power is restricted to 9 W and the volume is restricted to $(0.12\,\mathrm{m} \times 0.12\,\mathrm{m} \times 0.12\,\mathrm{m})$. In this work, the range is defined as the distance between the coils when the induced voltage drops to 1 mVpk or -60 $\mathrm{dB\,Vpk}$. The orientation of the coil is assumed to be near the worst case of 5° relative to the flux lines. Using this definition, a maximum sensing range of 400 mm is achieved at 220 kHz.

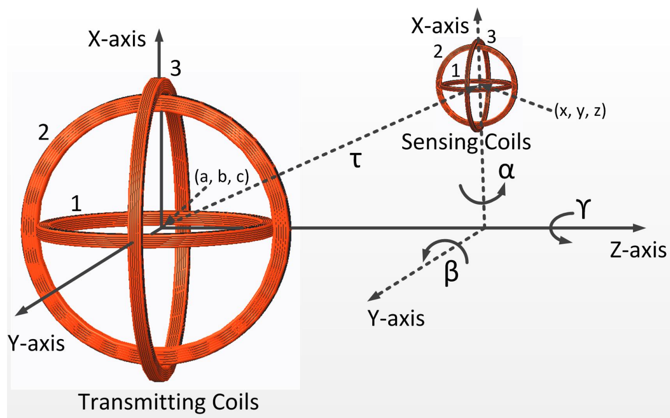

Fig. 1: A 6-DOF electromagnetic (EM) tracking system

In the next section, model for the induced voltage is derived. In section 3, the simulation and experimental results are presented. The transmitter optimization algorithm is described in section 4, then the paper is concluded in section 5.

II. Mathematical Analysis

A 6-DOF electromagnetic tracking system composed of concentric, orthogonal transmitting and sensing coils is shown in Fig. 1 [31]. The transmitting coils are energized to create magnetic dipoles parallel to the X-axis, Y-axis or Z-axis. The system parameters are summarized in Table I.

The magnetic flux density at any position (x, y, z) from the center of a transmitting coil (a, b, c) as shown in Fig. 1 can

TABLE I: Parameters of EM tracking system

G	Construction parameter which is equal to $(k_1 \times l_{tc} + k_2 \times r + k_3 \times t_c)$. The values of k_1, k_2 and k_3 are defined by Wheeler [30]. For a single turn coil, k_1 = 0 and k_3 = 0. For single layer coil, k_3 = 0.
$\vec{m}$	Total magnetic dipole moment of transmitting coils.
r	Radius of the transmitting coil.
t_c	Thickness of the transmitting coil.
l_{tc}	Length of the transmitting coil.
R_{tc}	Resistance of the transmitting coil.
X_{tc}	Inductive reactance of the transmitting coil.
C_{tc}	Self-capacitance of the transmitting coil.
V_a	Voltage applied to the transmitting coil.
N	Number of turns in the transmitting coil
ζ	Total turns-area of the sensing coil $(nA = \sum_{i=1}^{n} A_i)$
A	Area of the sensing coil.
μ_{tc}	Permeability of the core used in the transmitting coil.
μ_m	Permeability of the medium of the tracking system
D_{cu}	Diameter of the insulated wire used for transmitting coil.
D_c	Diameter of the wire used for the transmitting coil without insulation.
D_{core}	Inner diameter of the transmitting coil or the outer diameter of the core.
μ_{cu}	Permeability of the wire used for transmitting coil.
I_a	Current in transmitting coil.
V_{coil}	Voltage induced in the sensing coil
τ	Sensing range of the system

be written as [32].

$$\vec{B} = B_X \vec{i} + B_Y \vec{j} + B_Z \vec{k} = \frac{\mu}{4\pi}\left(\frac{3(\vec{m}.\vec{\tau})\vec{\tau}}{\tau^5} - \frac{\vec{m}}{\tau^3}\right) \quad (1)$$

where the distance vector $\vec{\tau} = [(x-a), (y-b), (z-c)]^T$, and the distance between the transmitter and the sensing coil is $\tau = \sqrt{(x-a)^2 + (y-b)^2 + (z-c)^2}$. $\vec{m} = (m_1, m_2, m_3)^T$, where m_1, m_2 and m_3 represent the magnetic dipole moments to the X, Y and Z-axes, respectively. The dipole moments are equal to $\pi N r_i^2 I_a$, where r_i represents the radius of the transmitting coils and $i = \{1, 2, 3\}$. From equation (1), the components of the magnetic flux density B at (x, y, z) are

$$B_X = \frac{\mu}{4\pi}\left\{\frac{3[m_1(x-a) + m_2(y-b) + m_3(z-c)](x-a)}{\tau^5} - \frac{m_1}{\tau^3}\right\} \quad (2)$$

$$B_Y = \frac{\mu}{4\pi}\left\{\frac{3[m_1(x-a) + m_2(y-b) + m_3(z-c)](y-b)}{\tau^5} - \frac{m_2}{\tau^3}\right\} \quad (3)$$

$$B_Z = \frac{\mu}{4\pi}\left\{\frac{3[m_1(x-a) + m_2(y-b) + m_3(z-c)](z-c)}{\tau^5} - \frac{m_3}{\tau^3}\right\} \quad (4)$$

Consider the transmitting coil of radius r that creates a magnetic dipole parallel to the X-axis, and a sensing coil at (x, y, z) as shown in Fig. 2. So, $\vec{m} = (m_1, 0, 0)^T$ and $m_1 = \pi N r^2 I_a$. Let the center of the transmitting coil be

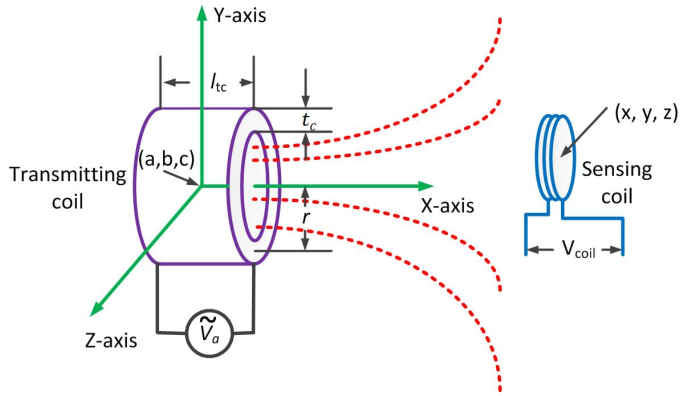

Fig. 2: Electromagnetic induction in the sensing coil due to a magnetic dipole which is parallel to the X-axis

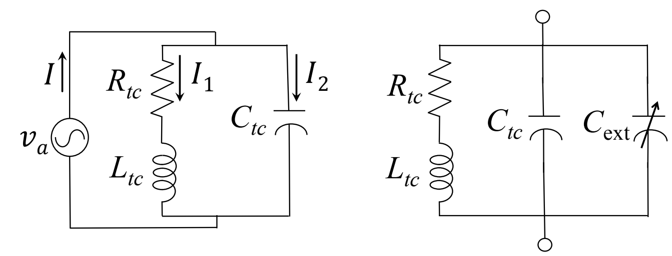

(a) (b)

Fig. 3: (a) Equivalent circuit of a transmitter (b) Circuit diagram to estimate C_{tc} by applying the resonance method.

(0, 0, 0). From equations (1), (2), (3) and (4), the magnetic flux density at (x, y, z) can be written as

$$B = \begin{bmatrix} B_X \\ B_Y \\ B_Z \end{bmatrix} = \Upsilon Q(x, y, z)\sin(\omega t), \quad (5)$$

where $Q(x, y, z)$ and Υ are introduced for notational simplicity, and are defined by

$$Q(x, y, z) = \frac{1}{\tau^5}\begin{bmatrix} 2x^2 - y^2 - z^2 \\ 3xy \\ 3xz \end{bmatrix} \quad (6)$$

and

$$\Upsilon = \frac{\mu_m}{4} N r^2 I_a \quad (7)$$

$$= \frac{\mu_m r^2 N}{4}\frac{V_a}{Z_{tc}}. \quad (8)$$

The equivalent circuit of a transmitting coil is shown in Fig.3. Let $Z_1 = \sqrt{R_{tc}^2 + X_{tc}^2}$, and $Z_c = 1/2\pi f C_{tc}$. Therefore, $Z_{tc} = Z_1 || Z_c$. R_{tc} and X_{tc} are the resistance and inductive reactance of the transmitting coil, respectively. Both R_{tc} and X_{tc} are functions of frequency. $R_{tc} = \frac{2rN}{D_{cu}}\left(\sqrt{\pi f \rho \mu_{cu} \mu_o}\right)$, $X_{tc} = \eta\frac{2\pi f N^2 r^2}{G}$ or $X_{tc} = \frac{2\pi^2 f \mu_{tc} N^2 r^2}{l_{tc}}$. The expression for G and the value of η can be found in the inductance formulas given by Wheeler [30]. For a single layer helical, spiral, and

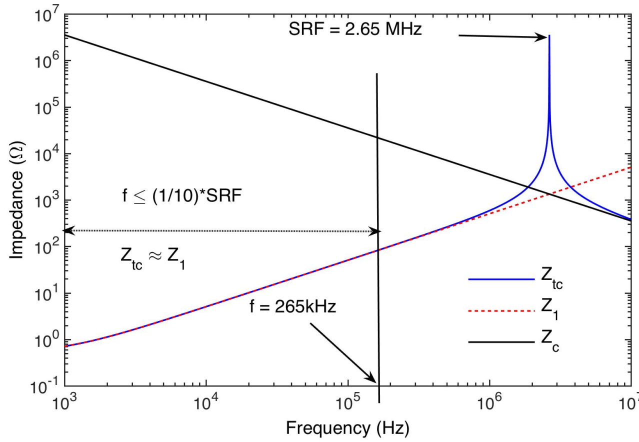

Fig. 4: Impedance characteristics of a transmitting versus frequency. L_{tc} = 80 μH, C_{tc} = 45 pF, SRF = 2.65 MHz

multi-layer coils, the values of G are $9r + 10l_{tc}$, $8r + 11t_c$ and $6r + 9l_{tc} + 10t_c$ and the values of η are 39.37×10^{-6}, 31.5×10^{-6} and 39.37×10^{-6}, respectively. C_{tc} also depends on the structure of the coil. The turn-turn capacitance can be calculated by [33]

$$C_{tt} = \epsilon_0 l_t \left[\frac{\epsilon_r \theta^*}{\ln\left(\frac{D_{cu}}{D_c}\right)} + \cot\left(\frac{\theta^*}{2}\right) - \cot\left(\frac{\pi}{12}\right) \right] \quad (9)$$

where, D_c is the diameter of the wire without insulation, ϵ_r is the relative permittivity of the insulation material, ϵ_0 = 8.85e-12, turn length $l_t = \pi * D_{core}$, $\theta^* = \arccos\left(1 - \left(\ln\left(D_{cu}/D_c\right)/\epsilon_r\right)\right)$, $N \geq 10$. The self-capacitance of the coil is $C_{tc} = \gamma C_{tt}$, where γ = 1.618 for a two-layer coil [33]. Experimentally the capacitance can be estimated by creating an electric resonance using an external capacitor, which is shown in Fig. 3b. Let the resonance frequencies are f_1 and f_2 for external capacitances C_{ext1} and C_{ext2}, respectively. The self-capacitance can be determined by,

$$C_{tc} = \frac{\left(\frac{f_2}{f_1}\right)^2 C_{ext2} - C_{ext1}}{1 - \left(\frac{f_2}{f_1}\right)^2} \quad (10)$$

The impact of signal frequency on the coil impedance is shown in Fig. 4. For frequencies less than or equal to one tenth of the self-resonance frequency (SRF), $Z_{tc} \approxeq Z_1$. In this frequency range, when $X_{tc} \gg R_{tc}$, the inductive reactance of a transmitting coil becomes approximately equal to it's impedance i.e., $X_{tc} \approx Z_{tc}$. Equation (8) can be written as

$$\Upsilon = \frac{V_a G \mu_m}{8\pi f \eta N} \quad (11)$$

or

$$\Upsilon = \frac{V_a \mu_m l_{tc}}{8\pi^2 f N \mu_{tc}} \quad (12)$$

Let the magnetic flux through the sensing coil be $\phi = BA'$, where A' is the area of the sensing coil. According to Faraday's and Lenz's laws, the induced voltage in the sensing coil at (x, y, z) is

$$\begin{aligned} V_{coil} &= -n\frac{d\phi}{dt} \\ &= -nA'\frac{dB}{dt} \\ &= -nA'\omega\Upsilon Q(x,y,z)\cos(\omega t) \\ &\quad [\text{ Substituting } B \text{ from (5)}] \end{aligned} \quad (13)$$

$$\Gamma(\alpha,\beta,\gamma) = \begin{bmatrix} \Gamma(1,1) & \Gamma(1,2) & \Gamma(1,3) \\ \Gamma(2,1) & \Gamma(2,2) & \Gamma(2,3) \\ \Gamma(3,1) & \Gamma(3,2) & \Gamma(3,3) \end{bmatrix} \quad (14)$$

The fractional area of the sensing coil perpendicular to ϕ varies with the rotation function $\Gamma(\alpha,\beta,\gamma)$. The angles α, β and γ are the rotation angles of the sensing coil about the X, Y and Z-axes, respectively. So, the fractional area is $A' = A\ \Gamma(\alpha,\beta,\gamma)$, where A is the cross-sectional area of the coil. $\Gamma(\alpha,\beta,\gamma)$ is given by where $\Gamma(1,1) = \cos(\beta)\cos(\gamma)$, $\Gamma(3,3) = \cos(\alpha)\cos(\beta)$, $\Gamma(2,1) = \cos(\gamma)\sin(\alpha)\sin(\beta) + \cos(\alpha)\sin(\gamma)$,
$\Gamma(3,1) = \sin(\alpha)\sin(\gamma) - \cos(\alpha)\cos(\gamma)\sin(\beta)$,
$\Gamma(1,2) = -\cos(\beta)\sin(\gamma)$, $\Gamma(2,3) = -\cos(\beta)\sin(\alpha)$,
$\Gamma(2,2) = \cos(\alpha)\cos(\gamma) - \sin(\alpha)\sin(\beta)\sin(\gamma)$,
$\Gamma(3,2) = \cos(\gamma)\sin(\alpha) + \cos(\alpha)\sin(\beta)\sin(\gamma)$,
$\Gamma(1,3) = \sin(\beta)$.

Therefore, the magnitude of the sensing voltage is

$$\begin{aligned} V_{coil} &= -nA\omega\Upsilon\Gamma(\alpha,\beta,\gamma)Q(x,y,z) \\ &= -\frac{V_a G \mu_m}{4\eta N}\zeta\Gamma(\alpha,\beta,\gamma)Q(x,y,z) \quad [\because \zeta = nA] \\ &= -\frac{V_a G \mu_m \zeta}{4\eta N}K \\ &= -F * K \end{aligned} \quad (15)$$

where

$$K = \begin{bmatrix} K_1 \\ K_2 \\ K_3 \end{bmatrix} = \Gamma(\alpha,\beta,\gamma)Q(x,y,z) \quad (16)$$

and

$$F = \frac{1}{4\eta} \times V_a \times \frac{G}{N} \times \zeta \times \mu_m \quad (17)$$

or based on (12), the equation for F can be written as

$$F = \frac{1}{4\pi} \times V_a \times \frac{1}{N} \times \frac{\mu_m}{\mu_{tc}} \times \zeta \times l_{tc} \quad (18)$$

K is a function of the position and orientation of the sensing coil. For a static sensing position, $V_{coil} \propto F$. From (17), the induced voltage depends on parameters such as the applied voltage and the dimensions of the transmitting and sensing coils. Therefore, to maximize the induced voltage, the transmitter dimensions and construction need to be optimized. It is also clear from (17) that the induced voltage does not vary with signal frequency. As the signal frequency increases, the magnitude of the flux density decreases but this is compensated by an increase in the rate of change $\frac{dB}{dt}$.

This article has been accepted for publication in a future issue of this journal, but has not been fully edited. Content may change prior to final publication. Citation information: DOI 10.1109/TMAG.2017.2703653, IEEE Transactions on Magnetics

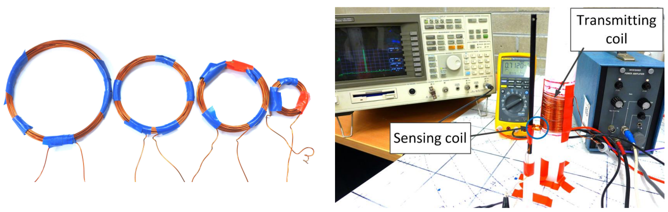

(a) (b)

Fig. 5: (a) Various transmitting coils used to test the impact of radius on induced voltage. (b) Experimental setup for testing the impact of signal frequency, current, voltage, and the number of turns in the transmitting coil on induced voltage.

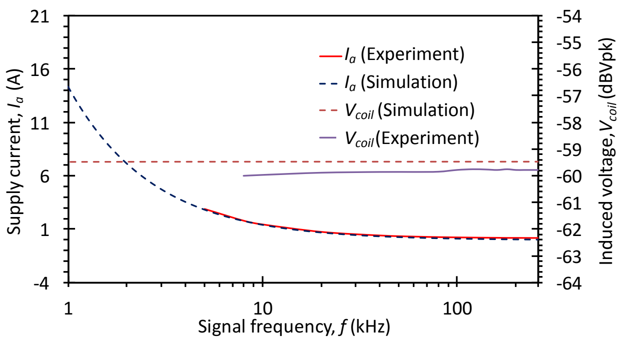

Fig. 6: Simulation and experimental results that illustrate the relationship between the induced voltage in the sensing coil and the signal frequency and current.

A. Condition to make $X_{tc} \gg R_{tc}$ or $X_{tc} \approx Z_{tc}$

The derived induced voltage is simplified by the condition,

$$\begin{aligned} X_{tc} &\gg R_{tc} \\ \eta \frac{2\pi f N^2 r^2}{G} &\gg \frac{2rN\sqrt{\pi f \rho \mu_{cu}}}{D_{cu}} \\ N\sqrt{f} &\gg \left(\frac{1}{\eta\sqrt{\pi}}\right) \times \left(\frac{G}{r}\right) \times \left(\frac{\sqrt{\rho\mu_{cu}}}{D_{cu}}\right) \end{aligned} \tag{19}$$

In order to satisfy this condition, the value of N and f should be high. The conductor should be as thick as possible with lowest possible resistivity and G should be minimized.

Equation (15) implies that an increased G and decreased N will increase the induced voltage and reduce the inductive reactance. Therefore, by increasing frequency, a greater voltage can be applied without increasing current, which increases the induced voltage.

III. Simulation and Experimental Analysis

In this section, the relationship between the induced voltage and the system parameters is experimentally verified. First, the invariance of induced voltage to frequency is verified. Then the impact of the applied voltage and dimensions of the transmitting coil are tested. The sensing coil used in the experiment is an air cored cylinder with a 2.5 mm length and 10 mm diameter. The sensing coil has 25 turns of 0.45 mm enamelled copper wire which results in a total turns-area ζ of 1950 turn.mm^2.

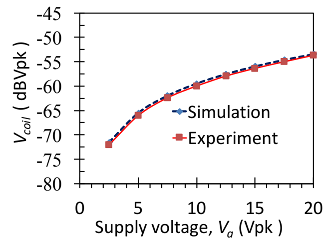

(a) $V_{coil} \propto V_a$

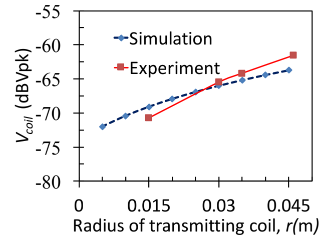

(b) $V_{coil} \propto r$

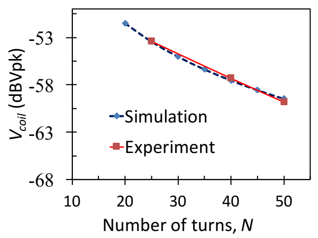

(c) $V_{coil} \propto \frac{1}{N}$

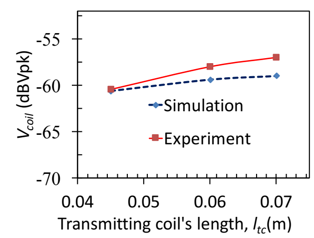

(d) $V_{coil} \propto l_{tc}$

Fig. 7: Variation of induced voltage in the sensing coil due to the variation of (a) applied voltage, (b) the radius of the transmitting coil, (c) the number of turns in the transmitting coil, and (d) the length of the transmitting coil.

The experimental setup is shown in Fig.5b. The single layer air cored transmitting coil is placed at (0,0,0) on the XY plane and the sensing coil is placed at (0.115 m, 0 m, 0.01 m). The orientation of the sensing coil is ($\alpha = 0°$, $\beta = 90°$, $\gamma = 0°$). The other parameters are $V_a = 10$ Vpk, $\zeta =$ 1950 turn.mm^2, $D_{cu} = 1 \times 10^{-3}$ m, $\mu_{cu} = 1.256629 \times 10^{-6}$ H/m, $D_c =$ 0.95 mm, N = 50, D_{core} = 48.5 mm, and $\rho = 1.68 \times 10^{-8}\ \Omega\,\mathrm{m}$. The experimentally determined parameters are L_{tc} = 80 μH, C_{tc} = 45 pF. Using (9), the calculated value of C_{tc} is 33 pF, which is close to the experimentally estimated value. The transmitting coil is energized by an AC signal and the induced voltage in the sensing coil was recorded.

In Figure 6 the induced voltage is observed to independent of frequency from 5 kHz to 160 kHz. On the other hand, the current reduces with the frequency as the impedance of the transmitting coil increases.

The experimental setup in Fig. 5b is also used to verify the impact of applied voltage and the number of turns on the induced voltage. In this experiment, the applied voltage is varied from 2.5 Vpk to 20 Vpk. Both simulation and experimental results are plotted in Fig. 7a. The induced voltage is observed to increase with supply voltage. While testing the impact of the number of turns, the length of the coil was 4 cm and the number of turns is varied from 25 to 50. The applied voltage and frequency were 10 Vpk and 43.5 kHz. The results are plotted in Fig. 7c. It can be observed that when the number of turns in the transmitting coil is increased, the induced voltage in the sensing coil decreases.

The relationship between the length of the transmitting coil and the induced voltage is also verified. This experiment also uses the setup shown in Fig. 5b. The length of a 50 turn coil with a radius of 0.025 m was varied from 0.04 m to 0.07 m. The transmitting coil is placed

This article has been accepted for publication in a future issue of this journal, but has not been fully edited. Content may change prior to final publication. Citation information: DOI 10.1109/TMAG.2017.2703653, IEEE Transactions on Magnetics

at (0,0,0) and the 6D position of the sensing coil was $(0.115\ \mathrm{m}, 0\ \mathrm{m}, 0.01\ \mathrm{m}, \alpha = 0°, \beta = 90°, \gamma = 0°)$. The simulation and experimental results are plotted in Fig. 7d. The induced voltage is approximately proportional to the transmitting coil length. The discrepancy between the simulated and experimental results is due to the approximate nature of Wheeler's formula.

The voltage induced in the sensing coil also depends on the radius of the transmitting coil. In order to verify this relation, the radius of the transmitting coil is varied from $15\ \mathrm{mm}$ to $46\ \mathrm{mm}$, as shown in Fig. 5a. The experimental setup is shown in Fig. 5b. The 6D position and orientation of the sensing coil was $(0.115\ \mathrm{m}, 0\ \mathrm{m}, 0.03\ \mathrm{m}, \alpha = 0°, \beta = 90°, \gamma = 0°)$. The induced voltage in the sensing coil is plotted in Fig. 7b. The induced voltage is approximately proportional to the transmitter radius. The discrepancy between the simulation and experimental results is due to the approximate nature of Wheeler's approximation.

IV. Transmitter Optimization

A 6-DOF localization system can be constructed from several combinations of transmitting and sensing coils, such as multiple coplanar transmitting coils and one sensing coil [17], [18], [34] or an LC marker [14], [15], [19]; two transmitting and three sensing coils [3], [4] or three transmitting and two sensing coils [5]. The transmitting and sensing coils could be arranged in different ways, such as coplanar [18], [34], collocated, orthogonal, or non planar and non-collocated [35]. In a tracking system, the orthogonal and concentric arrangement of transmitting coils [5]–[8] or sensing coils [3], [4], [10] is preferred due the simplification provided by the shared center points. Due to the simplicity and ease of construction, this configuration is used almost exclusively in the literature unless application requirements prevent it [36]. Therefore, the orthogonal and concentric arrangement is the only configuration considered in this article.

A. Transmitting Coil Modeling

The transmitting coil can be designed with a single or multilayer structure. In this article each of the transmitting coils are considered to be multilayer. Three concentric, orthogonal transmitting coils are shown in Fig. 8a. These coils are placed on the YZ, ZX and XY planes respectively and create magnetic fields parallel to the X, Y and Z axes. Let the diameters of the three coils be D_1, D_2, and D_3, and the lengths be l_1, l_2 and l_3.

Coil 1 exists from $-X$ to $+X$, where $X = l_1/2$. The coil is air cored and cylindrical in shape. To explain the dimensions of the three coils in Fig. 8a, an imaginary cuboid is shown in Fig.8b which exists inside the innermost coil. The height and depth of the cuboid are equal to d_1. The maximum length of the coil is the length of the cuboid. The diameter of coil 1 can then be written as

$$D_1 = \sqrt{2}d_1 + t_c \tag{20}$$

Assume the maximum length of coil 1 is equal to the height or depth of the cuboid

$$l_{1max} = d_1 \tag{21}$$

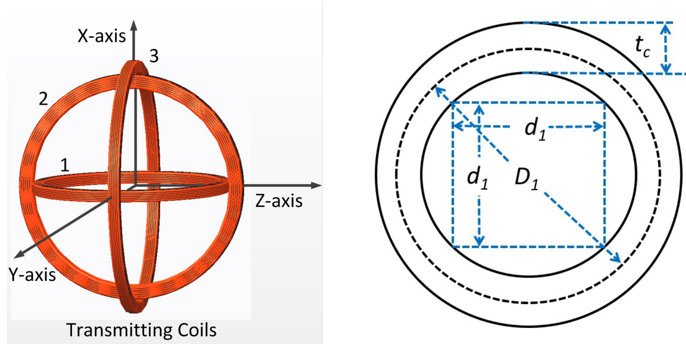

(a) (b)

Fig. 8: (a) Concentric, orthogonal transmitting coils, and (b) the cross-sectional view of the innermost coil.

TABLE II: Parameters for an example endoscope capsule localization system

Maximum transmitting power, P_{max}	9 W (15 Vpk, 0.6 A)
Volume of transmitter	10 cm × 10 cm × 10 cm
Transmitting coil's wire diameter, D_{cu}	1 mm
Total turns area of sensing coil, ζ	15200 turns.mm^2
SNR required at sensing coil	30 dB
Noise Figure, NF	-90 dB

Coil 2 exists from $-Y$ to $+Y$, where $Y = l_2/2$. Therefore, the diameter of coil 2 is

$$D_2 = \sqrt{(d_2^2 + l_1^2)} + t_c \tag{22}$$

where $d_2 = D_1 + t_c$ and the maximum length of coil 2 is

$$l_{2max} = d_2 = \sqrt{2}l_1 + 2t_c \tag{23}$$

Coil 3 exists from $-Z$ to $+Z$, where $Z = l_3/2$. The diameter of coil 3 is

$$D_3 = \sqrt{(d_3^2 + l_2^2)} + t_c \tag{24}$$

where $d_3 = D_2 + t_c$ and the maximum length of the coil is

$$l_{3max} = d_3 = \sqrt{\left(\sqrt{2}l_1 + 2t_c\right)^2 + l_1^2} + 2t_c \tag{25}$$

Let the length of each side of a cubic space restricted by the application be T, determined by

$$\begin{aligned} T &= D_3 + t_c \\ &= \left(\sqrt{\left(2t_c + \sqrt{(\sqrt{2}d_1 + 2t_c)^2 + l_1^2}\right)^2 + l_2^2}\right) + 2t_c \end{aligned} \tag{26}$$

The above equations are verified by PTC Creo parametric.

B. Algorithm Analysis

The input parameters for the algorithm are the: length of the restricted cubic space, maximum power P_{max}, frequency f, NF, SNR and ζ. The steps of the algorithm are summarized in Algorithm 1.

This article has been accepted for publication in a future issue of this journal, but has not been fully edited. Content may change prior to final publication. Citation information: DOI 10.1109/TMAG.2017.2703653, IEEE Transactions on Magnetics

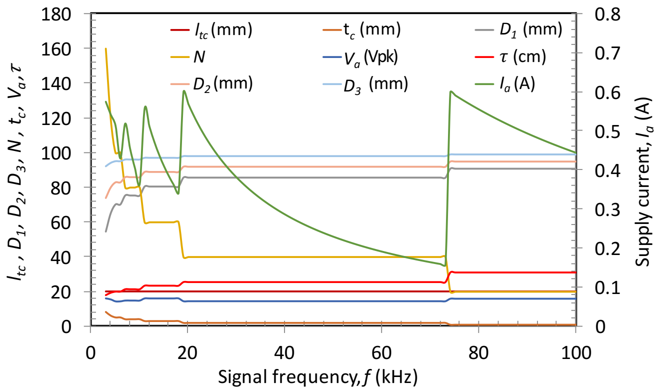

Fig. 9: Optimized transmitting coil dimensions when the length of the transmitting coils is fixed at 20 mm. The values at 74.1 kHz are considered to be optimal since the transmitting coil is single layer and the sensing range τ is maximum at that frequency.

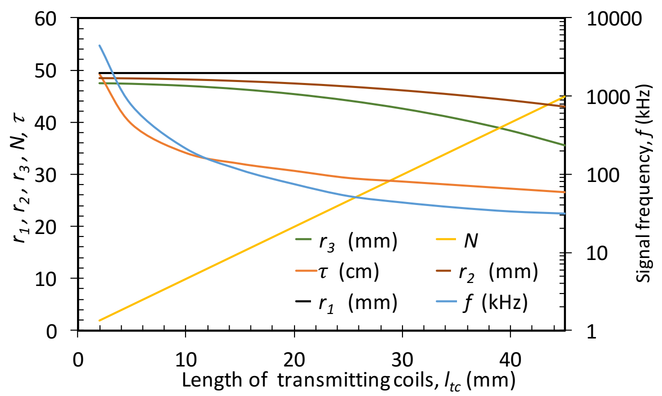

Fig. 10: Optimized transmitting coil dimensions as a function of length, and the achievable sensing ranges τ at different signal frequencies. V = 15 Vpk, I = 0.6 A, t_c = 1 mm, l_{tc} = 1 $\sim$ 45 mm. The radius of the transmitting coils are r_1, r_2 and r_3.

The algorithm will be demonstrated on the example endoscope parameters listed in Table II. The center of the transmitting coils is considered to be at (0, 0, 0). The initial position of the sensing coil is at (0.13 m, 0.07 m, 0.06 m), which is then moved by 0.002 m steps in all directions. The orientation of the sensing coil, which is perpendicular to the X-axis, is (α = 5 °, β = 5 °, γ = 5°). The desired induced voltage at full range is V_{coil} = -60 dB Vpk or 1 mVpk.

Fig. 9 shows the optimal coil dimensions when the length of the transmitting coil is fixed at 20 mm. In the figure, the values at 74.1 kHz are considered optimal since the transmitting coil is single layer at that frequency and the sensing range τ is maximized.

Fig.10 shows the optimal coil dimensions as a function of length, from 1 $\sim$ 40 mm. The single-layer transmitting coil is most efficient which occurs at minimum length.

To examine the impact of applied voltage on the measurement range, the algorithm is executed for voltages of between 10 and 40 Vpk, with a fixing power. The results are shown

Algorithm 1 Algorithm to determine the transmitting coil's dimensions

Inputs: Width of each coil t_c, the length of the given cubic space O, maximum power P_{max} ($V_{a,max}$, $I_{s,max}$) and the frequency f, Noise floor (NF), SNR and ζ

Outputs: Optimized dimensions of the transmitting coil.

1: Calculate the required minimum voltage in the sensing coil V_{coil} as $V_{coil} = 10^{\left(\frac{NF+SNR}{20}\right)}$
2: Find the maximum d_1, which is multiple times of D_{cu}, that satisfies $T \approx O$.
3: Based on d_1 and t_c, calculate l_{1max}, l_{2max} and l_{3max} using (21), (23) and (25) respectively. Fix the value of l_1, l_2 and l_3, where $l_1 \leq l_{1max}$, $l_2 \leq l_{2max}$ and $l_3 \leq l_{3max}$. In order to make the design simple, consider l_1 = l_2 = l_3.
4: Determine D_1, D_2 and D_3.
5: Determine the measurement range for $V_{a,max}$ by shifting the sensing coil until it satisfies (15).
6: Calculate $N = \frac{l_1 \times t_c}{D_{cu}^2}$ and R_{tc}, X_{tc}, C_{tc}, Z_{tc} and $I_a = V_a/Z_{tc}$.
7: **if** $I_a <= I_{a,max}$ and $f \leq (1/10) * SRF$ **then**
8:     **go to** 13
9: **else**
10:     Increase t_c, or N ($\frac{l_1 \times t_c}{D_{cu}^2} \geq N$). Update all the dimensions.
11:     **go to** 5
12: **end if**
13: Print out parameters D_1, D_2, D_3, τ, t_c, N, l_1, l_2 and l_3.

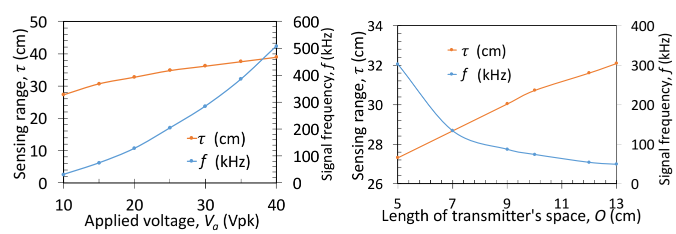

(a) $P = 9$ W, V_a = 10 $\sim$ 40 Vpk, l_{tc} = 20 mm, O = 10 cm

(b) P = 9 W, O = 5 $\sim$ 13 cm, l_{tc}= 20 mm, V_a = 15 Vpk

Fig. 11: The sensing range for optimal coil dimensions versus (a) applied voltage, and (b) enclosed transmitter volume.

in Fig. 11a. The improvement of sensing range at higher applied voltage is clearly observed. For a preexisting system, the range can be increased by increasing the applied voltage since $\tau_2 = \left(\frac{V_{a2}}{V_{a1}}\right)^{\frac{1}{3}} \times \tau_1$ where the frequency of the signal should be $f_2 = \left(\frac{V_{a2}}{V_{a1}}\right) \times f_1$ to maintain an identical current.

The improvement of measurement range due to increased transmitter volume can be observed in in Fig. 11b where O is varied from 5 $\sim$ 13 cm. Since the inductance of the transmitter increases with diameter, a reduced frequency is required to maintain a current constant.

The impact of the transmitting coil width t_c on the range is plotted in Fig. 12. When the number of layers in the transmitting coil is reduced, the diameter of the coil can be increased. For example, a single layer coil has the maximum diameter. Due to the proportional relationship of induced voltage with the

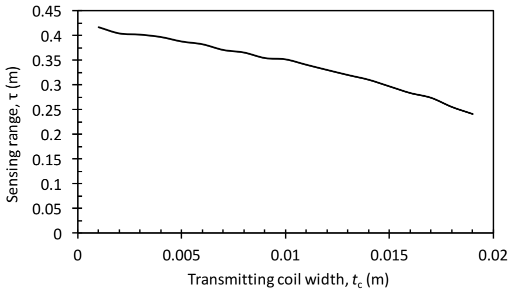

Fig. 12: The relationship between the transmitting coil width and system range.

diameter as shown in Fig. 7b, the sensing range increases with a decrease in t_c. Therefore, a single layer transmitting coil provides better range than a multilayer coil.

C. Example Comparison

To illustrate the possible improvements in range that can be achieved by optimizing the transmitter coil construction, the following example compares a naively constructed coil to an optimized coil. The transmitting coil former under consideration has a radius of 39 mm, a length of 20 mm and a maximum width of 4 mm. Using 0.9 mm diameter wire, the available volume permits 60 turns in 4 layers. With a driving frequency of 9 kHz, a 7.07 Vrms source results in 0.3 Arms, which is an apparent power of 2.1 VA. Using the endoscope capsule described in Table II, the induced voltage reduces to 1 mVpk at a range of 225 mm (when orthogonal to the transmitter).

By following the proposed optimization procedure, a single layer coil of 20 turns is found to be optimal. To maintain an apparent power of 2.1 VA, a 33 kHz driving signal resulted in the same voltage and current. The sensing range was extended from 225 mm to 310 mm.

Therefore, by optimizing the coil geometry, a 37% improvement in range is achieved. Although it is not possible to generalize this comparison, it is a useful illustration of the performance gains that are achievable. Although some of the optimal construction and operation parameters are obvious, others are less so, or even counter-intuitive, which motivates the use of the proposed algorithm.

V. Conclusion

This article describes an algorithm for optimizing the dimensions of transmitting coils in electromagnetic tracking applications. The restrictions considered include the applied signal power, frequency, and available volume. Simulation results are verified by experiments which illustrate the impact of transmitter dimensions on the magnitude of induced voltage. The key findings were:

- Single layer transmitting coils provide maximum induced voltage for a given transmitter power.
- When the applied voltage is constant, the signal frequency or applied power does not affect the induced voltage. Conversely, the induced voltage can be increased by increasing the induced voltage.
- Increasing the transmitter volume increases the induced voltage.

Therefore, to maximise the induced voltage, it is desirable to maximize the applied voltage, radius and length of the transmitting coil, while minimizing the number of turns.

Maximizing the induced voltage is particularly important in applications with a limited sensor volume, such as capsule endoscopy, electronic pills, and catheter tracking. The sensitivity and range of these application can be maximized by the proposed method.

References

[1] F. H. Raab, E. B. Blood, T. O. Steiner, and H. R. Jones, "Magnetic position and orientation tracking system," *Aerospace and Electronic Systems, IEEE Transactions on*, no. 5, pp. 709–718, 1979.

[2] M. Li, S. Song, C. Hu, D. Chen, and M.-H. Meng, "A novel method of 6-dof electromagnetic navigation system for surgical robot," in *Intelligent Control and Automation (WCICA), 2010 8th World Congress on*. IEEE, 2010, pp. 2163–2167.

[3] E. Paperno, I. Sasada, and E. Leonovich, "A new method for magnetic position and orientation tracking," *Magnetics, IEEE Transactions on*, vol. 37, no. 4, pp. 1938–1940, 2001.

[4] S. Song, C. Hu, B. Li, X. Li, and M.-H. Meng, "An electromagnetic localization and orientation method based on rotating magnetic dipole," *Magnetics, IEEE Transactions on*, vol. 49, no. 3, pp. 1274–1277, 2013.

[5] J. Tian, S. Song, X. Wang, T. Yan, C. Hu, and M.-H. Meng, "An improved method and algorithm for electromagnetic localization," in *Information and Automation (ICIA), 2011 IEEE International Conference on*. IEEE, 2011, pp. 406–411.

[6] S. Song, W. Qiao, B. Li, C. Hu, H. Ren, and M. Q.-H. Meng, "An efficient magnetic tracking method using uniaxial sensing coil," *IEEE Transactions on Magnetics*, vol. 50, no. 1, pp. 1–7, 2014.

[7] S. Song, H. Ren, and H. Yu, "An improved magnetic tracking method using rotating uniaxial coil with sparse points and closed form analytic solution," *IEEE Sensors Journal*, vol. 14, no. 10, pp. 3585–3592, 2014.

[8] W. Ashe, "System and method for magnetic position tracking," Jan. 2 2014, uS Patent App. 13/534,666. [Online]. Available: http://www.google.com/patents/US20140002063

[9] W. Wang, C. Hu, W. Lin, and J. Bao, "An improved pso-based algorithm for extracting week coupling ac signal in electromagnetic localization system," in *Automation and Logistics (ICAL), 2012 IEEE International Conference on*. IEEE, 2012, pp. 623–627.

[10] J. Kuipers, "Tracking and determining orientation of object using coordinate transformation means, system and process," Sep. 28 1976, uS Patent 3,983,474. [Online]. Available: http://www.google.com.au/patents/US3983474

[11] A. Govari, "Electromagnetic position single axis system," Nov. 19 2002, uS Patent 6,484,118.

[12] Y. Zhigang and Y. Kui, "An improved 6dof electromagnetic tracking algorithm with anisotropic system parameters," in *Technologies for E-Learning and Digital Entertainment*. Springer, 2006, pp. 1141–1150.

[13] I. Aoki, A. Uchiyama, K. Arai, K. Ishiyama, and S. Yabukami, "Detecting system of position and posture of capsule medical device," Oct. 19 2010, uS Patent 7,815,563.

[14] S. Hashi, S. Yabukami, H. Kanetaka, K. Ishiyama, and K. Arai, "Numerical study on the improvement of detection accuracy for a wireless motion capture system," *Magnetics, IEEE Transactions on*, vol. 45, no. 6, pp. 2736–2739, 2009.

[15] S. Hashi, S. Yabukami, H. Kanetaka, K. Ishiyama, and K. I. Arai, "Wireless Magnetic Position-Sensing System Using Optimized Pickup Coils for Higher Accuracy," *IEEE Transactions on Magnetics*, vol. 47, no. 10, pp. 3542–3545, Oct. 2011.

[16] R. Graumann, "Cable-free endoscopy method and system for determining in vivo position and orientation of an endoscopy capsule," Aug. 25 2005, uS Patent App. 11/015,357. [Online]. Available: http://www.google.com/patents/US20050187479

[17] X. Guo, C. Wang, and R. Yan, "An electromagnetic localization method for medical micro-devices based on adaptive particle swarm optimization with neighborhood search," *Measurement*, vol. 44, no. 5, pp. 852–858, Jun. 2011.

[18] X.-d. Guo, G.-z. Yan, and P.-p. Jiang, "Feasibility of localizing in vivo micro-devices with electromagnetic methods," *Journal of Shanghai Jiaotong University (Science)*, vol. 13, no. 5, pp. 559–561, Nov. 2008.

This article has been accepted for publication in a future issue of this journal, but has not been fully edited. Content may change prior to final publication. Citation information: DOI 10.1109/TMAG.2017.2703653, IEEE Transactions on Magnetics

[19] M. Bechtold, C. Gabriel, and A. Juloski, "Arrangement and method for navigating an endoscopic capsule," May 2 2013, uS Patent App. 13/458,937. [Online]. Available: https://www.google.com/patents/US20130109920

[20] T. Nagaoka and A. Uchiyama, "Development of a small wireless position sensor for medical capsule devices," in *Engineering in Medicine and Biology Society, 2004. IEMBS'04. 26th Annual International Conference of the IEEE*, vol. 1. IEEE, 2004, pp. 2137–2140.

[21] http://polhemus.com/.

[22] http://www.ascension-tech.com/.

[23] www.razerzone.com/.

[24] X. Guo, C. Song, and R. Yan, "Optimization of multilayer cylindrical coils in a wireless localization system to track a capsule-shaped micro-device," *Measurement*, vol. 46, no. 1, pp. 117–124, jan 2013.

[25] S. Tumanski, "Induction coil sensorsa review," *Measurement Science and Technology*, vol. 18, no. 3, p. R31, 2007.

[26] P. Anderson, "Electromagnetic tracking method and system," Mar. 8 2011, uS Patent 7,902,817. [Online]. Available: http://www.google.com.au/patents/US7902817

[27] M. A. Nixon, B. C. McCallum, W. R. Fright, and N. B. Price, "The effects of metals and interfering fields on electromagnetic trackers," *Presence: Teleoperators and Virtual Environments*, vol. 7, no. 2, pp. 204–218, 1998.

[28] V. V. Kindratenko, "A survey of electromagnetic position tracker calibration techniques," *Virtual Reality*, vol. 5, no. 3, pp. 169–182, 2000.

[29] P. Sharma and S. Guha, "Transmission of time varying magnetic field through body tissue," *Journal of Biological Physics*, vol. 3, no. 2, pp. 95–102, 1975.

[30] H. A. Wheeler, "Simple inductance formulas for radio coils," *Radio Engineers, Proceedings of the Institute of*, vol. 16, no. 10, pp. 1398–1400, 1928.

[31] M. N. Islam and A. J. Fleming, "A novel and compatible sensing coil for a capsule in wireless capsule endoscopy for real time localization," in *SENSORS, 2014 IEEE*, Nov 2014, pp. 1607–1610.

[32] D. K. Cheng, "Field and wave electromagnetics static magnetic," *Addison Wesley Publishing*, 1989.

[33] A. Massarini and M. K. Kazimierczuk, "Self-capacitance of inductors," *IEEE Transactions on Power Electronics*, vol. 12, no. 4, pp. 671–676, 1997.

[34] A. Plotkin and E. Paperno, "3-d magnetic tracking of a single subminiature coil with a large 2-d array of uniaxial transmitters," *Magnetics, IEEE Transactions on*, vol. 39, no. 5, pp. 3295–3297, 2003.

[35] M. Schneider, "Measuring position and orientation using magnetic fields," Jun. 6 2000, uS Patent 6,073,043. [Online]. Available: http://www.google.com/patents/US6073043

[36] http://sixense.com/wireless.

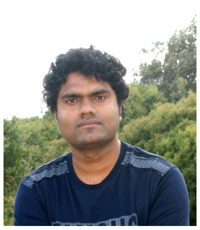

Mohd Noor Islam received his B.Sc in Electrical & Electronic Engineering from Khulna University of Engineering and Technology, Khulna, Bangladesh in 2003. He has completed his M.Sc in Electronic Engineering from Kookmin University, Seoul, Korea in 2009. He had been teaching as a Lecturer and then as an Assistant Professor in the Department of Electrical and Electronic Engineering in Khulna University of Engineering and Technology since 2004. Now he is pursuing his PhD in Electrical Engineering in the school of Electrical Engineering and Computer Science in the University of Newcastle, Callaghan, Australia. His research interests are implanted devices and their communications, Electromagnetic localization, robotic endoscope capsule etc.

Dr. Andrew Fleming graduated from The University of Newcastle, Australia with a Bachelor of Electrical Engineering in 2000 and Ph.D in 2004. Dr. Fleming is now an Australian Research Council Future Fellow and Director of the Precision Mechatronics Lab at The University of Newcastle, Australia. His research includes nanofabrication, micro-robotics, meteorological sensing, nano-positioning, and high-speed scanning probe microscopy. Dr. Flemings research awards include the IEEE Transactions on Control Systems Technology Outstanding Paper Award, The University of Newcastle Researcher of the Year Award, and the Faculty of Engineering and Built Environment Award for Research Excellence. He is the co-author of three books and more than one-hundred Journal and Conference papers. Dr. Fleming is the inventor of several patent applications and in 2012 he received the Newcastle Innovation Rising Star Award for Excellence in Industrial Engagement.